Leakage and slow allostery limit performance of single drug-sensing aptazyme molecules based on the hammerhead ribozyme

CHAMAREE DE SILVA[1] and NILS G. WALTER[2]

[1]Biophysics, University of Michigan, Ann Arbor, Michigan 48109-1055, USA
[2]Department of Chemistry, Single Molecule Analysis Group, University of Michigan, Ann Arbor, Michigan 48109-1055, USA

ABSTRACT

Engineered "aptazymes" fuse in vitro selected aptamers with ribozymes to create allosteric enzymes as biosensing components and artificial gene regulatory switches through ligand-induced conformational rearrangement and activation. By contrast, activating ligand is employed as an enzymatic cofactor in the only known natural aptazyme, the *glmS* ribozyme, which is devoid of any detectable conformational rearrangements. To better understand this difference in biosensing strategy, we monitored by single molecule fluorescence resonance energy transfer (FRET) and 2-aminopurine (AP) fluorescence the global conformational dynamics and local base (un)stacking, respectively, of a prototypical drug-sensing aptazyme, built from a theophylline aptamer and the hammerhead ribozyme. Single molecule FRET reveals that a catalytically active state with distal Stems I and III of the hammerhead ribozyme is accessed both in the theophylline-bound and, if less frequently, in the ligand-free state. The resultant residual activity (leakage) in the absence of theophylline contributes to a limited dynamic range of the aptazyme. In addition, site-specific AP labeling shows that rapid local theophylline binding to the aptamer domain leads to only slow allosteric signal transduction into the ribozyme core. Our findings allow us to rationalize the suboptimal biosensing performance of the engineered compared to the natural aptazyme and to suggest improvement strategies. Our single molecule FRET approach also monitors in real time the previously elusive equilibrium docking dynamics of the hammerhead ribozyme between several inactive conformations and the active, long-lived, Y-shaped conformer.

Keywords: RNA conformational change; aminopurine fluorescence; single molecule FRET; structural dynamics

INTRODUCTION

Riboswitches represent a recently discovered gene regulatory paradigm wherein binding of a small-molecule metabolite to an RNA motif embedded in the 5′ or 3′ untranslated region of a pre-mRNA controls gene expression via transcription, translation, or alternative splicing (Breaker 2004; Mandal and Breaker 2004; Winkler and Breaker 2005; Coppins et al. 2007; Serganov and Patel 2007; Wakeman et al. 2007; Montange and Batey 2008). Expression of an estimated 2%–3% of all bacterial genes and an unknown number of eukaryotic genes is controlled in this economic protein-free fashion (Mandal and Breaker 2004; Winkler and Breaker 2005; Wakeman et al. 2007). Ligand binding to a riboswitch is thought, typically, to induce an RNA conformational change by either kinetic or thermodynamic control that affects an adjacent expression platform (Al-Hashimi and Walter 2008). A notable exception is the *glmS* catalytic riboswitch, or aptazyme, located upstream of the *glmS* gene of Gram-positive bacteria (Mandal and Breaker 2004; Winkler et al. 2004; Winkler and Breaker 2005). It employs its glucosamine-6-phosphate (GlcN6P) ligand as a chemical cofactor (McCarthy et al. 2005) in a self-cleavage reaction that causes mRNA degradation (Collins et al. 2007), without the involvement of any detectable conformational change (Hampel and Tinsley 2006; Klein and Ferré-D'Amaré 2006; Cochrane et al. 2007; Tinsley et al. 2007).

In pioneering work initiated years before naturally occurring riboswitches were discovered, artificial aptazymes were engineered for use as biosensor components and artificial genetic switches by fusing an in vitro selected aptamer to a naturally occurring ribozyme, affording a ligand dependent RNA conformational change as a mechanism that activates

the ribozyme motif (Breaker 2002, 2004; Silverman 2003; Blount et al. 2006; Mayer and Famulok 2006; Hall et al. 2007; Wieland and Hartig 2008; Win and Smolke 2008). In a prototypical such biosensor aptazyme, a theophylline-specific aptamer is incorporated via a communication module into Stem II of the hammerhead ribozyme (Fig. 1A; Soukup and Breaker 1999; Breaker 2002; Sekella et al. 2002), the smallest known natural catalytic RNA (Milligan and Uhlenbeck 1989; Salehi-Ashtiani and Szostak 2001; Blount and Uhlenbeck 2005; Nelson and Uhlenbeck 2008). Theophylline binding activates the ribozyme, leading to cleavage of a substrate strand in *cis* or *trans*, depending on strand connectivity, which in turn can be coupled to a radioactive (Breaker 2002) or fluorescent signal (Sekella et al. 2002; Rueda and Walter 2006). Theophylline, or dimethylxanthine (Fig. 1B), is a bronchodilating drug used in therapy for respiratory diseases including asthma, bronchitis, and emphysema. It is characterized by a narrow therapeutic range of between ∼55 and 110 μM in blood plasma, with numerous side effects above this range, necessitating that an administered dose be closely monitored (Hendeles and Weinberger 1983; Miyazawa et al. 2002). The theophylline aptamer was previously in vitro selected to have micromolar ligand affinity and to discriminate 10,000-fold against the ubiquitous, structurally similar caffeine (Fig. 1B; Jenison et al. 1994; Zimmermann et al. 2000; Sekella et al. 2002), making it an attractive aptazyme component. Yet in tests of its dynamic range, an important quality of molecular tools in analytical applications (Mairal et al. 2008), the theophylline aptazyme falls about three orders of magnitude short (Soukup and Breaker 1999; Sekella et al. 2002) of the 100,000-fold ligand-induced activation observed for the naturally occurring *glmS* aptazyme (Winkler et al. 2004; McCarthy et al. 2005).

To further optimize engineered aptazymes for use as biosensor components (Breaker 2002) and RNA-based switches for controlling gene expression (Wieland and Hartig 2008; Win and Smolke 2008), it is critical to understand the weaknesses of existing aptazyme designs. Here we probe the allosteric mechanism of the prototypical theophylline aptazyme by single molecule and ensemble fluorescence spectroscopy. We find that the engineered aptazyme is characterized by leaky and slow conformational changes, rationalizing the superior performance of the cofactor-activated *glmS* aptazyme. Our findings lead us to suggest specific strategies for improvement of artificial engineered aptazymes.

RESULTS

The prototypical theophylline-dependent aptazyme shows limited dynamic range and significant background cleavage in the absence of ligand

We previously developed an ensemble fluorescence resonance energy transfer (FRET) assay for the theophylline
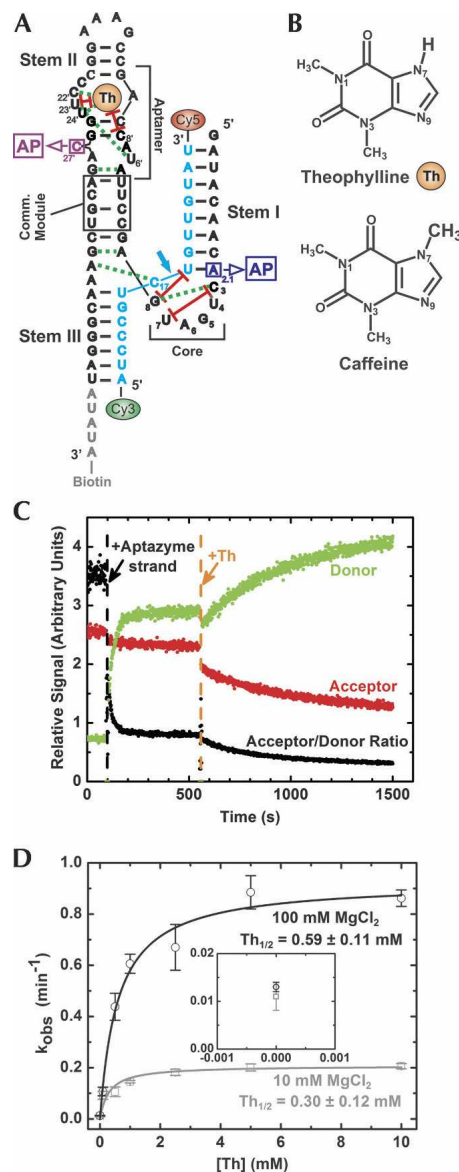
FIGURE 1. Theophylline aptazyme used in this study. (*A*) The assembled aptazyme (black) and substrate strands (cyan), forming Stems I, II, and III and the aptamer, communication, and catalytic core domains as indicated with canonical numbering schemes. The substrate is labeled with a FRET donor (Cy3) and acceptor (Cy5), and its cleavage site is indicated by an arrow. The aptazyme strand is 3′-biotinylated for surface immobilization during smFRET experiments. Theophylline (Th) ligand binding to the aptamer domain is probed by substituting either C27′ or A2.1 with AP as indicated. Important hydrogen bond and stacking interactions as observed by X-ray crystallography (Martick and Scott 2006) are indicated as green dashed and red solid lines, respectively. (*B*) Chemical structures of theophylline and caffeine. (*C*) Steady-state ensemble fluorescence signals of the FRET labeled cleavable substrate upon sequential addition of aptazyme strand and 10 mM theophylline (Th) under our standard conditions of 50 mM Tris-HCl (pH 7.5), 25 mM DTT, 100 mM MgCl$_2$, at 25°C. (*D*) Theophylline concentration dependence of the cleavage rate constants derived from single-exponential fits to acceptor/donor ratio time courses like that in panel *C*, yielding the indicated theophylline half-titration points, Th$_{1/2}$, at 10 mM and 100 mM MgCl$_2$ (Materials and Methods). The *inset* zooms in on the rate constants in the absence of theophylline.

aptazyme where a 5′-donor (Cy3) and 3′-acceptor (Cy5) labeled substrate (which positions the fluorophores into Stems III and I, respectively, of the hammerhead ribozyme) (Fig. 1C) is cleaved in *trans*, leading to a conveniently monitored FRET decrease upon theophylline addition (Sekella et al. 2002; Rueda and Walter 2006). We utilize this assay here to measure a dynamic range for theophylline detection as a key indicator of biosensor performance (Mairal et al. 2008) that is quite modest, consistent with earlier studies (Soukup and Breaker 1999; Sekella et al. 2002): We observe an ∼20-fold increase in cleavage activity between 0 and 10 mM theophylline at 10 mM MgCl$_2$, which increases to ∼70-fold at 100 mM MgCl$_2$ (Fig. 1D). This dynamic range does not measure up to that of the naturally occurring *glmS* aptazyme, which shows an ∼100,000-fold activity increase between 0 and 10 mM GlcN6P (Winkler et al. 2004; McCarthy et al. 2005). Notably, a significant background ("leakage") cleavage rate constant of 0.013 min^{-1} is observed in the absence of theophylline (100 mM MgCl$_2$, which we define as our standard conditions henceforth; inset of Fig. 1D) and confirmed by radioactive cleavage assays (Sekella et al. 2002; data not shown), which drastically limits the dynamic range (calculated as a fold increase relative to the background reaction).

Single molecule FRET reveals distinct global conformational isomers

We hypothesized that the cause for the modest performance of the theophylline aptazyme compared to the naturally occurring *glmS* ribozyme may be linked to the fact that a ligand-induced conformational change is required for the theophylline aptazyme, while none is found in the natural aptamer (Hampel and Tinsley 2006; Klein and Ferré-D'Amaré 2006; Cochrane et al. 2007; Tinsley et al. 2007). To test this hypothesis and probe for global conformational changes upon ligand binding in the absence of dynamics caused by catalysis, we studied the aptazyme by single molecule FRET (smFRET) in the presence of a noncleavable 2′-*O*-methyl substrate modification at the cleavage site (C17) (Fig. 1A). Fluorescence of Cy3 and Cy5 on the 5′ and 3′ ends of the substrate strand, respectively, was monitored in real time using prism-based total internal reflection fluorescence microscopy (TIRFM) on surface immobilized aptazymes, essentially as described (Zhuang et al. 2002; Pereira et al. 2008; Walter et al. 2008). Attachment of the smFRET donor–acceptor pair to Stems I and III (Fig. 1A) was the same as for our ensemble cleavage assays (Fig. 1C) and chosen based on previous ensemble FRET studies of the hammerhead ribozyme suggesting that Stems I and III are proximal in an inactive conformation, but become distal upon Mg^{2+} titration and catalytic activation (Bassi et al. 1999; Rueda et al. 2003; Penedo et al. 2004). Indeed,

smFRET time trajectories reveal anti-correlated changes in the donor and acceptor signals in the presence of 10 mM theophylline (which is saturating as judged from the activity titration in Fig. 1D), with states of high (H, ∼0.8) and low (L, ∼0.2) smFRET (Fig. 2A). Observation
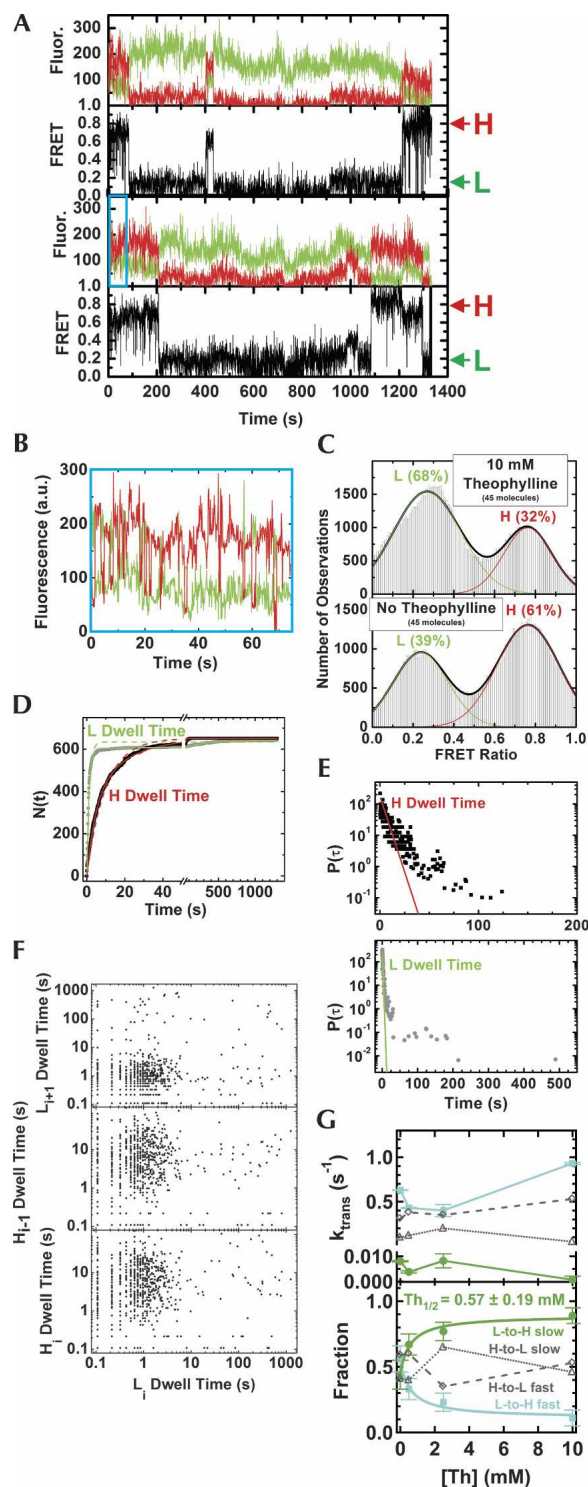

FIGURE 2. (Legend on next page)

of an H state is consistent with a global conformation in which Stems I and III come into close proximity (below the Förster distance of Cy3 and Cy5 of ~54 Å) (Sabanayagam et al. 2005), while the L state is consistent with a large distance between the two stems (well beyond the Förster distance). The fact that these H and L states are readily detected and persist for seconds to minutes at a time suggests that they are structurally quite stable and well defined. smFRET thus uncovers the existence of an equilibrium distribution of previously unobserved, distinct conformational isomers in a hammerhead ribozyme with either proximal or distal Stems I and III.

Single aptazymes access pairs of high and low smFRET states of distinct kinetic behavior

Aptazymes switch between the H and L states with kinetics that are well resolved at the single molecule level (Fig. 2A). A prominent long-lived L state is observed in many trajectories, while molecules that are in the H state take frequent but brief excursions to the L state (Fig. 2B). An aggregate smFRET histogram of 45 molecules underscores the resulting preference (68%) for time spent in the L state while in the presence of 10 mM theophylline (Fig. 2C). Notably, a similar bimodal smFRET distribution is observed in the absence of theophylline (also 45 molecules), although with a less abundant L state (39%, Fig. 2C). Histograms of different subsets of molecules produce similar results (data not shown). The equilibrium shift toward the L state upon addition of theophylline leads us to hypothesize that this state is associated with the observed ligand-induced catalytic activation.

Rate constants for interconversion of the H to the L state and vice versa in the presence of 10 mM theophylline are

deduced from cumulative plots of all single molecule dwell times in the H and L states, respectively (Fig. 2D). Double exponentials are required to fit both sets of dwell times (Fig. 2D also shows the best single-exponential fits for comparison), in accord with the heterogeneous behavior of single molecules over extended time periods in Figure 2A. The deviation from simple single-exponential kinetics is further highlighted by plotting the probability density functions (Fig. 2E). The rate constants from the cumulative dwell time plots are corrected for photobleaching and observation time limitations as previously described (Rueda et al. 2004). The resulting pair of H-to-L transition rate constants ($0.21 \ sec^{-1}$ and $0.05 \ sec^{-1}$; approximately a fourfold difference) are less distinct from one another than those characterizing the L-to-H transition ($0.93 \ sec^{-1}$ and $0.0007 \ sec^{-1}$; ~1300-fold difference), consistent with the qualitative observation that a very short-lived and a very long-lived L state coexist in single molecule trajectories (Fig. 2A). Notably, we observe no correlation (memory) between either consecutive L state dwell times or between the L and adjacent H state dwell times (Fig. 2F), further suggesting that each molecule can freely access each of the underlying four states (two H, two L states) without stochastic bias from its preceding behavior. Similar observations of four rate constants and associated states extend to conditions of low and zero theophylline (Fig. 2G).

Catalytic activity is associated with the long-lived low smFRET state

The corrected H-to-L and L-to-H transition rate constants are shown in Figure 2G (top panel) over varying theophylline concentrations. The bottom panel of Figure 2G shows the relative fractional amplitudes of the transitions (adding up to unity), as calculated from the exponential fits to the cumulative dwell time histograms (see Materials and Methods). All rate constants and the relative fractional amplitudes of the H-to-L rate constants vary little and/or show no consistent trend. By contrast, the fractional amplitude of the slower L-to-H transition significantly increases with the theophylline concentration (bottom panel, green curve) while the faster L-to-H fractional amplitude decreases (bottom panel, cyan curve), observations that are consistent with an increasing dominance of the long-lived L state as evidenced in the aggregate smFRET histogram of Figure 2C. Global fitting of the two L-to-H fractional amplitudes yields a theophylline half-titration point of $Th_{1/2} = 0.57 \pm 0.19$ mM, within error identical to the $Th_{1/2}$ value (0.59 ± 0.11 mM) of catalytic activation under the same conditions (Fig. 1D;100 mM $MgCl_2$). This identity strongly supports a link between catalytic activity and specifically the long-lived L state. We propose that this long-lived L state encompasses the conformationally docked active state of the hammerhead-derived theophylline aptazyme, which forms the expected (Blount and

FIGURE 2. smFRET analysis of the theophylline aptazyme. (*A*) Representative smFRET time traces of two aptazyme molecules (*top* and *bottom* pairs of plots) under standard conditions in the presence of 10 mM theophylline. The raw Cy3 donor and Cy5 acceptor fluorescence signals are green and red, respectively, and the corresponding smFRET ratio $[I_A/(I_A + I_D)]$ is shown in black with the observed H and L states indicated. (*B*) Expanded portion from the cyan box in panel *a*, showing rapid conformational changes within the molecule. (*C*) Aggregate smFRET histograms in the presence and absence of 10 mM theophylline. (*D*) Cumulative dwell time histograms of the L and H smFRET states for calculating the L-to-H and H-to-L transition rate constants, respectively, and their corresponding fractions at 10 mM theophylline (Materials and Methods). (*E*) Probability density plots for the H and L state dwell times. The steep decay portions were fit with single exponentials (colored lines) to highlight deviations thereof at 10 mM theophylline. (*F*) Plots of the immediately following L state dwell time (L_{i+1}) as well as immediately following and preceding H dwell times (H_{i+1} and H_i, respectively) as a function of a given L dwell time L_i at 10 mM theophylline. (*G*) Corrected transition rate constants (*top*) and their corresponding fractions (*bottom*) as deduced from cumulative dwell time histograms similar to the one shown in panel *D* (Materials and Methods). The fractions of the two L-to-H rate constants were fit globally to obtain the indicated theophylline half-titration point $Th_{1/2}$.

Uhlenbeck 2005; Nelson and Uhlenbeck 2008) Y-shape with distal Stems I and III (Fig. 1A), while the H states represent undocked, catalytically inactive conformations.

Site-specific 2-aminopurine fluorescence probing provides evidence for slow allosteric signal transduction

To also probe for local conformational changes in the aptamer and catalytic core domains, we substituted the fluorescent adenine analog 2-aminopurine (AP) for the nonconserved C27′ and A2.1 residues, respectively, in separate aptazyme mutants (Fig. 1A). Using either stopped-flow or manual mixing combined with steady-state fluorescence detection, changes in AP fluorescence as a probe for local base stacking interactions (Gondert et al. 2006) were monitored upon addition of varying theophylline concentrations. As expected, the AP fluorescence increases in the aptamer (C27′ → AP) mutant upon addition of 10 mM theophylline (Fig. 3A, upper panel) since nucleotide 27′ (Fig. 1A) becomes solvent exposed in the ligand-bound aptamer (Jucker et al. 2003). By contrast, the AP fluorescence decreases in the core (A2.1 → AP) mutant upon 10 mM theophylline addition (Fig. 3A, lower panel), presumably due to increased base stacking of the core around the U1.1–AP2.1 base pair (Fig. 1A; Menger et al. 1996).

The kinetics of the structural rearrangement detected by AP in the aptamer and core mutants are strikingly different (Fig. 3). The rate constant of the local conformational change in the aptamer domain, as measured in the aptamer mutant, becomes as fast as 63 sec^{-1} at saturating theophylline concentrations, only about sevenfold slower than in the isolated aptamer (Jucker et al. 2003). The observed saturation behavior with $Th_{1/2} < 0.1$ mM suggests that under these conditions the conformational change, not theophylline binding, is rate limiting (Fig. 3B). Notably, the conformational changes in the catalytic core, detected in the core mutant, occur at a much slower rate constant of at most 0.08 sec^{-1} under saturating (rate-limiting) conditions ($Th_{1/2} = 1.6 \pm 0.8$ mM; Fig. 3B). That is, the conformational change induced in the catalytic core near the cleavage site of the aptazyme by distal theophylline binding (Fig. 1A) is ~800-fold slower than the structural rearrangement in the theophylline binding aptamer itself. These observations suggest that signal transduction by conformational rearrangements from the aptamer domain through the communication module to the catalytic core is relatively slow, limiting the maximal cleavage output of the aptazyme. This upper limit further reduces the attainable dynamic range (ratio of maximal activity over background cleavage) of the aptazyme as a biosensor for theophylline.

DISCUSSION

Recently, engineered aptazymes have been found to be of interest as biosensor components (Breaker 2002) and as RNA devices for cellular information processing (Wieland and Hartig 2008; Win and Smolke 2008). Here, we have used single molecule FRET to observe in real time the global dynamics between Stems I and III of a drug-sensing hammerhead-derived aptazyme, indicating that the active conformation docks into a Y-shape. Ligand binding to the aptamer domain incorporated into Stem II favors a long-lived, catalytically active docked state, revealing the ligand-induced conformational activation mechanism of the aptazyme. This same docked state is also visited, albeit less frequently, in the absence of ligand, accounting for both the observed background activity (leakage) and part of the limited dynamic range of sensing. Together with the observation from specific 2-aminopurine labeling that allosteric signal transduction from the aptamer to the catalytic core is slow, our results suggest that the designs of this and other biosensing aptazymes can be further improved to match the performance of nature's only known aptazyme, the *glmS* ribozyme.

Despite extensive studies since the mid-1980s, details on the structural dynamics of the hammerhead ribozyme have remained elusive until now. Our data reveal that at equilibrium an aptazyme designed based on the hammerhead ribozyme fluctuates between several inactive conformations and the active, expectedly Y-shaped (Blount and Uhlenbeck 2005; Nelson and Uhlenbeck 2008) conformer.
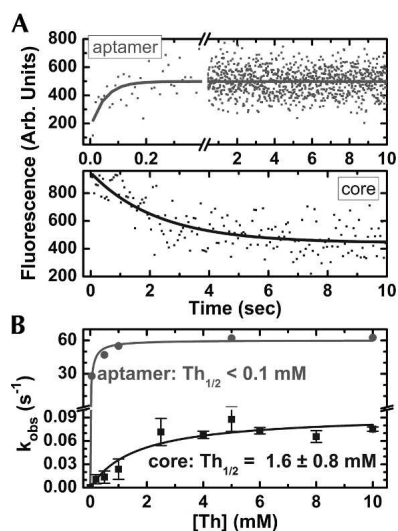
FIGURE 3. Fluorescence changes upon addition of 10 mM theophylline to AP labeled aptazymes. (*A*) Increasing AP fluorescence signal of the aptamer (C27′ → AP) mutant (*top*) and decreasing AP fluorescence signal of the catalytic core (A2.1 → AP) mutant (*bottom*). (*B*) Theophylline concentration dependence of the theophylline binding rate constants derived from single-exponential fits to AP fluorescence time courses like those in panels *A* and *B*, yielding the indicated theophylline half-titration points, $Th_{1/2}$, for the aptamer and core mutants (Materials and Methods).

As evident from Figure 2, our smFRET probing specifically suggests that (1) A pair of H (high smFRET) states as well as a pair of L (low smFRET) states exist that are distinguished by their dwell times (Fig. 2A,B,D,E), but not their smFRET values, as the histograms of Figure 2C show close-to-ideal bimodal distributions with no evidence for additional states of distinct smFRET value. (2) It is the particularly long-lived L state with distal Stems I and III whose prevalence correlates with catalytic activity (Fig. 1, cf. D and G). (3) Each single molecule can freely interchange between all four states, that is, the heterogeneity described here exists between pairs of structurally yet not kinetically, similar H and L states that dynamically exchange for any given molecule without memory of any preceding behavior (Fig. 2F). This behavior is distinct from that described for the similarly small hairpin ribozyme, where distinct subpopulations of molecules exist that do not interconvert on any experimentally accessible timescale (Zhuang et al. 2002; Bokinsky et al. 2003; Okumus et al. 2004; Rueda et al. 2004; Ditzler et al. 2008).

Our AP fluorescence probing highlights the fact that the aptamer domain is relatively unperturbed by incorporation into the aptazyme, as solvent exposure of nucleotide position $27'$ upon theophylline binding still occurs and is only sevenfold slower (Fig. 3B) than without appended ribozyme (Jucker et al. 2003). Yet, coupling of the ligand-induced, localized conformational changes of the aptamer domain through the communication domain into the catalytic core of the hammerhead ribozyme motif (Fig. 1A) is ∼800-fold slower (Fig. 3B), suggesting that a significant energetic barrier of ∼4 kcal/mol, equivalent to the breaking of several hydrogen bonds, has to be overcome in this long-range structural communication. Such a significant barrier is consistent with the "slippage" mechanism proposed to be responsible for properly aligning a base pair in the communication domain upon ligand binding (Soukup and Breaker 1999; Breaker 2002; Hall et al. 2007). Our findings suggest that the design or in vitro selection of aptazymes with such a barrier has been inherently limiting the achievable dynamic range and response time of a biosensor.

Figure 4 schematically shows the simplest kinetic reaction pathway consistent with all our data. Each molecule switches between two high and two low smFRET states that are distinguished by their dwell time kinetics. The low smFRET state characterized by a very slow conversion back to a high smFRET state can also spontaneously, but very slowly, reach a catalytically active conformation that generates cleavage product in the absence of theophylline ligand ("leakage pathway"). Rapid local binding of theophylline to the aptamer domain stabilizes a conformation that slowly rearranges the catalytic core into the active state to generate product ("biosensing pathway"). We here have determined the ratio of the overall rate constants through the biosensing and leakage pathways as <100-fold (Fig.

1D), which significantly limits the inherent dynamic range of the engineered biosensing aptazyme.

Engineered aptazymes based on the hammerhead ribozyme were first developed before the discovery of the natural *glmS* aptazyme (Soukup and Breaker 1999; Breaker 2002). Nature chose the GlcN6P ligand to act as a chemical participant of the *glmS* aptazyme reaction (McCarthy et al. 2005), contributing general acid (or possibly base) capacity so that ligand binding and catalytic activation can quickly and efficiently occur without the need for a conformational change (Hampel and Tinsley 2006; Klein and Ferré-D'Amaré 2006; Cochrane et al. 2007; Tinsley et al. 2007). By contrast, the hammerhead ribozyme is thought to utilize two of its own guanines (and possibly bound water molecules) for acid–base catalysis (Han and Burke 2005; Martick and Scott 2006; Walter 2007), making design of a ligand-induced, activating conformational change necessary to afford ligand dependence. We show here that single molecules of the prototypical theophylline aptazyme exhibit four global conformational states that are readily distinguished by the extent of smFRET between Stems I and III as well as their interconversion kinetics. We identify two drawbacks that limit the dynamic range of the aptazyme as a biosensor component: (1) leakage, i.e., significant residual activity in the ligand-free state and (2) slow allostery, i.e., slow transduction of the ligand binding signal from the aptamer to the catalytic core domain.
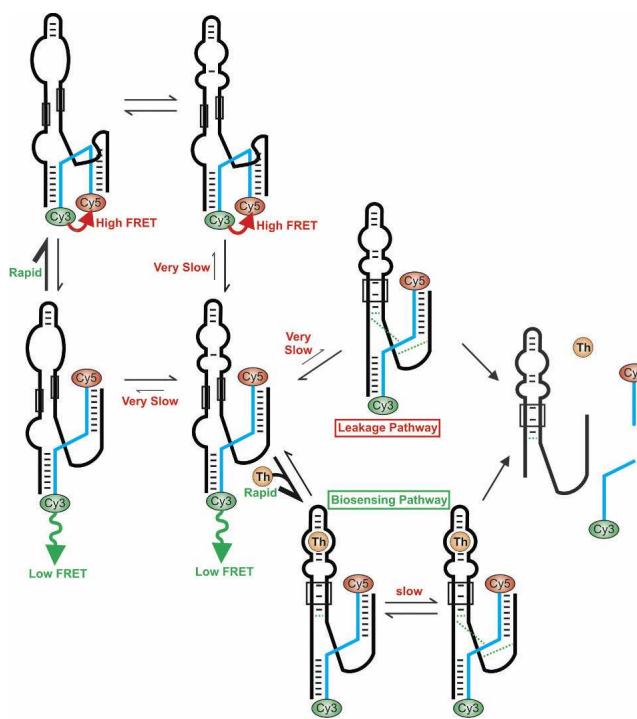
FIGURE 4. Proposed simplest kinetic pathway of the theophylline aptazyme consistent with our cleavage activity, smFRET, and AP fluorescence data.

While similar studies of other engineered aptazymes will need to follow to show the generality of our findings on the prototypical theophylline aptazyme, our results suggest three clear strategies to improve aptazyme performance: (1) Design aptazymes with a similar mode of action as the *glmS* ribozyme, i.e., where the ligand is used as a chemical cofactor. This strategy will of course be limited to certain types of ligands with chemically active functional groups. (2) Prevent the leakage reaction by more stringent selection against aptazymes that cleave in the absence of ligand without a loss in ligand-induced activity. (3) Facilitate (accelerate) signal transduction from the aptamer to the catalytic core domain by lowering the associated energetic barrier. This latter strategy may be implemented, for example, by designing aptamer domains that more fully envelop the ligand for a maximum gain in binding free energy, as observed in naturally occurring riboswitches (Batey et al. 2004; Serganov et al. 2004; Serganov and Patel 2007; Montange and Batey 2008). This enhanced binding free energy could then be harvested to more fully, and possibly more rapidly, rearrange the catalytic core into an active conformation. The future (combinatorial) exploration of such design strategies promises to overcome the limitations of currently available aptazymes for use as biosensor components and artificial genetic switches.

MATERIALS AND METHODS

RNA preparation

The aptazyme strand (Fig. 1A) was in vitro transcribed using T7 RNA polymerase from a single-stranded DNA template with double-stranded promoter purchased from Invitrogen and purified by denaturing polyacrylamide gel electrophoresis (D-PAGE) (Milligan and Uhlenbeck 1989). For smFRET the transcribed aptazyme strand was 3′-biotinylated by oxidization with periodate and reaction with biotin hydrazide as described (Newby Lambert et al. 2006). The chemically synthesized substrate and two AP modified aptazyme strands were purchased from the Keck Foundation Biotechnology Resource Laboratory at the Yale University School of Medicine, deprotected as recommended by the manufacturer, and purified by D-PAGE and C_8 reverse phase HPLC as described (Walter 2002). In all single-molecule FRET and AP-fluorescence based structure probing experiments a noncleavable substrate analog with a 2′-*O*-methyl modification at the cleavage site (C17) was employed. For all FRET experiments the substrate was labeled with Cy3 and Cy5 on the 5′ and 3′ ends during and after synthesis (the latter by coupling the dye succinimidyl ester to a C7 3′-Amino-Modifier), respectively, and repurified by C_8 reverse phase HPLC as described (Walter 2002).

Steady-state and stopped-flow ensemble fluorescence assays

Steady-state ensemble cleavage assays monitored by FRET were performed on an Aminco-Bowman 2 spectrofluorometer at 25°C in standard buffer (50 mM Tris-HCl at pH 7.5, 25 mM DTT) with either 10 mM or 100 mM $MgCl_2$ as indicated. We added 200 nM aptazyme to 50 nM cleavable substrate (both final concentrations) in the cuvette, and reactions were initiated by addition of theophylline to varying final concentrations as previously described (Rueda and Walter 2006). Theophylline binding kinetics were monitored by AP fluorescence of an annealed complex of 100 nM AP labeled aptazyme mutant and 400 nM noncleavable substrate analog (without fluorophores) at 25°C in standard buffer with 100 mM $MgCl_2$ in an SF-2001 stopped-flow spectrofluorometer (KinTek Corp.) fitted with a 75-W Xe-arc lamp. AP was excited at 315 nm (4 nm slit width), and its fluorescence was monitored using a 340-nm long-pass filter. Time traces of acceptor/donor signal ratio and of AP fluorescence were analyzed by least-squares fitting single exponentials to the data using Microcal Origin 7.0 software. The obtained rate constants were plotted against the theophylline concentration ($[Th]$) and fit with a hyperbolic, noncooperative binding equation of the form

$$k_{\mathrm{obs}} = k_{\max} \frac{[Th]}{[Th] + Th_{1/2}},$$

where $k_{\max}$ is the cleavage rate at saturating theophylline concentration and $Th_{1/2}$ is the theophylline half-titration point.

smFRET assays

The 3′-biotinylated aptazyme strand (500 nM final concentration) was annealed with the noncleavable Cy3/Cy5 doubly labeled substrate strand (1 μM) in standard buffer at 70°C for 2 min and cooled on ice for 15 min. The assembled RNA complex was diluted to 50 pM in standard buffer with 100 mM $MgCl_2$, supplemented with an oxygen scavenger system to prolong the lifetime of the fluorophores as described (Rueda et al. 2004), and bound at 25°C to a streptavidin coated quartz slide surface within a microfluidic channel as described (Ha 2001) until a density of ∼0.1 molecules/μm^2 was reached. A home-built prism-based total internal reflection fluorescence (TIRF) microscope with intensified CCD camera (I-PentaMAX, Roper Scientific Inc.) was used to observe the donor (I_D) and acceptor (I_A) fluorescence signals and the resulting smFRET ratio of $I_A/(I_A + I_D)$ at 100-msec time resolution, essentially as described (Pereira et al. 2008; Roy et al. 2008; Walter et al. 2008). The dwell times of all L and H states of each trajectory were calculated and cumulative dwell time histograms plotted and fit (using Microcal Origin 7.0) with double exponentials to obtain transition rate constants k_{trans} after correction for photobleaching and observation time limitations as described (Zhuang et al. 2002; Rueda et al. 2004). Using the amplitudes of the double-exponential fits, fractions of each observed L-to-H and H-to-L rate constant were calculated after also correcting for photobleaching and observation time limitations (Rueda et al. 2004). The theophylline concentration ($[Th]$) dependence of the fast and slow L-to-H fractions f (which add up to unity) were globally fit with a hyperbolic, noncooperative binding equation of the form

$$f = f_0 + (-1)^a f_{\max} \frac{[Th]}{[Th] + Th_{1/2,\,\mathrm{global}}},$$

where $a = 0$ leads to an increasing and $a = 1$ to a decreasing curve, f_0 and $f_{\max}$ characterize the start and end points of the two

titrations, respectively, and $Th_{1/2, \text{global}}$ is the common theophylline half-titration point.

Aggregate histograms of the counts of video frames with a specific smFRET value from each one of 45 representative molecules were plotted and fit with double Gaussians to calculate the percentage of time spent in the L and H states. We generated a continuous probability density plot of the dwell time data by weighing each event by the average time between its nearest neighbor events. This procedure has negligible impact on the short dwell times that are characterized by multiple events in each time bin, yet represents an improved statistical estimate of the probability density of long dwell times where the event density is low (Kuno et al. 2001). Dwell times of adjacent L and H states were also plotted against one another to detect correlations between them. Figure 2G was plotted using Igor Pro software, whereas all other plots were generated in Microcal Origin 7.0 software.

ACKNOWLEDGMENTS

REFERENCES

Al-Hashimi, H.M. and Walter, N.G. 2008. RNA dynamics: It is about time. *Curr. Opin. Struct. Biol.* **18:** 321–329.

Bassi, G.S., Mollegaard, N.E., Murchie, A.I., and Lilley, D.M. 1999. RNA folding and misfolding of the hammerhead ribozyme. *Biochemistry* **38:** 3345–3354.

Batey, R.T., Gilbert, S.D., and Montange, R.K. 2004. Structure of a natural guanine-responsive riboswitch complexed with the metabolite hypoxanthine. *Nature* **432:** 411–415.

Blount, K.F. and Uhlenbeck, O.C. 2005. The structure–function dilemma of the hammerhead ribozyme. *Annu. Rev. Biophys. Biomol. Struct.* **34:** 415–440.

Blount, K., Puskarz, I., Penchovsky, R., and Breaker, R. 2006. Development and application of a high-throughput assay for *glmS* riboswitch activators. *RNA Biol.* **3:** 77–81.

Bokinsky, G., Rueda, D., Misra, V.K., Rhodes, M.M., Gordus, A., Babcock, H.P., Walter, N.G., and Zhuang, X. 2003. Single-molecule transition-state analysis of RNA folding. *Proc. Natl. Acad. Sci.* **100:** 9302–9307.

Breaker, R.R. 2002. Engineered allosteric ribozymes as biosensor components. *Curr. Opin. Biotechnol.* **13:** 31–39.

Breaker, R.R. 2004. Natural and engineered nucleic acids as tools to explore biology. *Nature* **432:** 838–845.

Cochrane, J.C., Lipchock, S.V., and Strobel, S.A. 2007. Structural investigation of the *glmS* ribozyme bound to its catalytic cofactor. *Chem. Biol.* **14:** 97–105.

Collins, J.A., Irnov, I., Baker, S., and Winkler, W.C. 2007. Mechanism of mRNA destabilization by the *glmS* ribozyme. *Genes & Dev.* **21:** 3356–3368.

Coppins, R.L., Hall, K.B., and Groisman, E.A. 2007. The intricate world of riboswitches. *Curr. Opin. Microbiol.* **10:** 176–181.

Ditzler, M.A., Rueda, D., Mo, J., Håkansson, K., and Walter, N.G. 2008. A rugged free energy landscape separates multiple functional RNA folds throughout denaturation. *Nucleic Acids Res.* (in press).

Gondert, M.E., Tinsley, R.A., Rueda, D., and Walter, N.G. 2006. The catalytic core structure of the *trans*-acting HDV ribozyme is subtly influenced by sequence variation outside the core. *Biochemistry* **45:** 7563–7573.

Ha, T. 2001. Single-molecule fluorescence resonance energy transfer. *Methods* **25:** 78–86.

Hall, B., Hesselberth, J.R., and Ellington, A.D. 2007. Computational selection of nucleic acid biosensors via a slip structure model. *Biosens. Bioelectron.* **22:** 1939–1947.

Hampel, K.J. and Tinsley, M.M. 2006. Evidence for preorganization of the glmS ribozyme ligand binding pocket. *Biochemistry* **45:** 7861–7871.

Han, J. and Burke, J.M. 2005. Model for general acid–base catalysis by the hammerhead ribozyme: pH-activity relationships of G8 and G12 variants at the putative active site. *Biochemistry* **44:** 7864–7870.

Hendeles, L. and Weinberger, M. 1983. Theophylline. A "state of the art" review. *Pharmacotherapy* **3:** 2–44.

Jenison, R.D., Gill, S.C., Pardi, A., and Polisky, B. 1994. High-resolution molecular discrimination by RNA. *Science* **263:** 1425–1429.

Jucker, F.M., Phillips, R.M., McCallum, S.A., and Pardi, A. 2003. Role of a heterogeneous free state in the formation of a specific RNA–theophylline complex. *Biochemistry* **42:** 2560–2567.

Klein, D.J. and Ferré-D'Amaré, A.R. 2006. Structural basis of *glmS* ribozyme activation by glucosamine-6-phosphate. *Science* **313:** 1752–1756.

Kuno, M., Fromm, D.P., Hamann, H.F., Gallagher, A., and Nesbitt, D.J. 2001. "On"/"off" fluorescence intermittency of single semiconductor quantum dots. *J. Chem. Phys.* **115:** 1028–1040.

Mairal, T., Ozalp, V.C., Lozano Sanchez, P., Mir, M., Katakis, I., and O'Sullivan, C.K. 2008. Aptamers: Molecular tools for analytical applications. *Anal. Bioanal. Chem.* **390:** 989–1007.

Mandal, M. and Breaker, R.R. 2004. Gene regulation by riboswitches. *Nat. Rev. Mol. Cell Biol.* **5:** 451–463.

Martick, M. and Scott, W.G. 2006. Tertiary contacts distant from the active site prime a ribozyme for catalysis. *Cell* **126:** 309–320.

Mayer, G. and Famulok, M. 2006. High-throughput-compatible assay for *glmS* riboswitch metabolite dependence. *ChemBioChem* **7:** 602–604.

McCarthy, T.J., Plog, M.A., Floy, S.A., Jansen, J.A., Soukup, J.K., and Soukup, G.A. 2005. Ligand requirements for *glmS* ribozyme self-cleavage. *Chem. Biol.* **12:** 1221–1226.

Menger, M., Tuschl, T., Eckstein, F., and Porschke, D. 1996. Mg^{2+}-dependent conformational changes in the hammerhead ribozyme. *Biochemistry* **35:** 14710–14716.

Milligan, J.F. and Uhlenbeck, O.C. 1989. Synthesis of small RNAs using T7 RNA polymerase. *Methods Enzymol.* **180:** 51–62.

Miyazawa, Y., Starkey, L.P., Forrest, A., Schentag, J.J., Kamimura, H., Swarz, H., and Ito, Y. 2002. Effects of the concomitant administration of tamsulosin (0.8 mg/day) on the pharmacokinetic and safety profile of theophylline (5 mg/kg): A placebo-controlled evaluation. *J. Int. Med. Res.* **30:** 34–43.

Montange, R.K. and Batey, R.T. 2008. Riboswitches: Emerging themes in RNA structure and function. *Annu. Rev. Biophys.* **37:** 117–133.

Nelson, J.A. and Uhlenbeck, O.C. 2008. Hammerhead redux: Does the new structure fit the old biochemical data? *RNA* **14:** 605–615.

Newby Lambert, M., Vocker, E., Blumberg, S., Redemann, S., Gajraj, A., Meiners, J.C., and Walter, N.G. 2006. Mg^{2+}-induced compaction of single RNA molecules monitored by tethered particle microscopy. *Biophys. J.* **90:** 3672–3685.

Okumus, B., Wilson, T.J., Lilley, D.M., and Ha, T. 2004. Vesicle encapsulation studies reveal that single molecule ribozyme heterogeneities are intrinsic. *Biophys. J.* **87:** 2798–2806.

Penedo, J.C., Wilson, T.J., Jayasena, S.D., Khvorova, A., and Lilley, D.M. 2004. Folding of the natural hammerhead ribozyme is enhanced by interaction of auxiliary elements. *RNA* **10:** 880–888.

Pereira, M.J., Nikolova, E.N., Hiley, S.L., Jaikaran, D., Collins, R.A., and Walter, N.G. 2008. Single VS ribozyme molecules reveal dynamic and hierarchical folding toward catalysis. *J. Mol. Biol.* **382:** 496–509.

Roy, R., Hohng, S., and Ha, T. 2008. A practical guide to single-molecule FRET. *Nat. Methods* **5:** 507–516.

Rueda, D. and Walter, N.G. 2006. Fluorescent energy transfer readout of an aptazyme-based biosensor. *Methods Mol. Biol.* **335:** 289–310.

Rueda, D., Wick, K., McDowell, S.E., and Walter, N.G. 2003. Diffusely bound Mg^{2+} ions slightly reorient stems I and II of the hammerhead ribozyme to increase the probability of formation of the catalytic core. *Biochemistry* **42:** 9924–9936.

Rueda, D., Bokinsky, G., Rhodes, M.M., Rust, M.J., Zhuang, X., and Walter, N.G. 2004. Single-molecule enzymology of RNA: Essential functional groups impact catalysis from a distance. *Proc. Natl. Acad. Sci.* **101:** 10066–10071.

Sabanayagam, C.R., Eid, J.S., and Meller, A. 2005. Using fluorescence resonance energy transfer to measure distances along individual DNA molecules: Corrections due to nonideal transfer. *J. Chem. Phys.* **122:** 061103.

Salehi-Ashtiani, K. and Szostak, J.W. 2001. In vitro evolution suggests multiple origins for the hammerhead ribozyme. *Nature* **414:** 82–84.

Sekella, P.T., Rueda, D., and Walter, N.G. 2002. A biosensor for theophylline based on fluorescence detection of ligand-induced hammerhead ribozyme cleavage. *RNA* **8:** 1242–1252.

Serganov, A. and Patel, D.J. 2007. Ribozymes, riboswitches, and beyond: Regulation of gene expression without proteins. *Nat. Rev. Genet.* **8:** 776–790.

Serganov, A., Yuan, Y.R., Pikovskaya, O., Polonskaia, A., Malinina, L., Phan, A.T., Hobartner, C., Micura, R., Breaker, R.R., and Patel, D.J. 2004. Structural basis for discriminative regulation of gene expression by adenine- and guanine-sensing mRNAs. *Chem. Biol.* **11:** 1729–1741.

Silverman, S.K. 2003. Rube Goldberg goes (ribo)nuclear? Molecular switches and sensors made from RNA. *RNA* **9:** 377–383.

Soukup, G.A. and Breaker, R.R. 1999. Engineering precision RNA molecular switches. *Proc. Natl. Acad. Sci.* **96:** 3584–3589.

Tinsley, R.A., Furchak, J.R., and Walter, N.G. 2007. *Trans*-acting *glmS* catalytic riboswitch: Locked and loaded. *RNA* **13:** 468–477.

Wakeman, C.A., Winkler, W.C., and Dann 3rd, C.E. 2007. Structural features of metabolite-sensing riboswitches. *Trends Biochem. Sci.* **32:** 415–424.

Walter, N.G. 2002. Probing RNA structural dynamics and function by fluorescence resonance energy transfer (FRET). *Curr. Protoc. Nucleic Acid Chem.* **11.10:** 11.10.11–11.10.23.

Walter, N.G. 2007. Ribozyme catalysis revisited: Is water involved? *Mol. Cell* **28:** 923–929.

Walter, N.G., Huang, C.Y., Manzo, A.J., and Sobhy, M.A. 2008. Do-it-yourself guide: How to use the modern single-molecule toolkit. *Nat. Methods* **5:** 475–489.

Wieland, M. and Hartig, J.S. 2008. Improved aptazyme design and in vivo screening enable riboswitching in bacteria. *Angew. Chem. Int. Ed. Engl.* **47:** 2604–2607.

Win, M.N. and Smolke, C.D. 2008. Higher-order cellular information processing with synthetic RNA devices. *Science* **322:** 456–460.

Winkler, W.C. and Breaker, R.R. 2005. Regulation of bacterial gene expression by riboswitches. *Annu. Rev. Microbiol.* **59:** 487–517.

Winkler, W.C., Nahvi, A., Roth, A., Collins, J.A., and Breaker, R.R. 2004. Control of gene expression by a natural metabolite-responsive ribozyme. *Nature* **428:** 281–286.

Zhuang, X., Kim, H., Pereira, M.J., Babcock, H.P., Walter, N.G., and Chu, S. 2002. Correlating structural dynamics and function in single ribozyme molecules. *Science* **296:** 1473–1476.

Zimmermann, G.R., Wick, C.L., Shields, T.P., Jenison, R.D., and Pardi, A. 2000. Molecular interactions and metal binding in the theophylline-binding core of an RNA aptamer. *RNA* **6:** 659–667.